Scholars' Mine

Spring 2016

Iron phosphide nanostructures as an efficient bifunctional catalysts for water splitting

Nikitaa Ashokan

IRON PHOSPHIDE NANOSTRUCTURES AS AN EFFICIENT BIFUNCTIONAL

CATALYSTS FOR WATER SPLITTING

by

NIKITAA ASHOKAN

A THESIS

Presented to the Graduate Faculty of the

MISSOURI UNIVERSITY OF SCIENCE AND TECHNOLOGY

In Partial Fulfillment of the Requirements for the Degree

MASTERS

in

CHEMICAL ENGINEERING

2016

Approved by:

Dr. Xinhua Liang, Advisor
Dr. Manashi Nath, Co-Advisor
Dr. Sutapa Barua

PUBLICATION THESIS OPTION

This thesis consists of the following article that has been submitted for publication as follows: Pages 14-27 have been submitted to Journal of Materials Chemistry A.

This thesis follows formatting rules as set forth by the Missouri University of Science and Technology.

ABSTRACT

The first part of this thesis work focuses on developing a bifunctional catalyst for electrochemical water splitting encompassing both oxygen and hydrogen evolution. A highly efficient catalyst is necessary to improve kinetics of the sluggish four electron process for oxygen evolution reaction (OER) and two-electron process for hydrogen evolution reaction (HER). Recently, transition metal phosphides have gained increasing interest in this field because of their good electrical conductivity properties as well as better catalytic activity. Many transition-metal phosphides are being considered for this application and iron phosphide (FeP) has proved to be a good HER catalyst. In this work, we will discuss that FeP can also be used as an OER catalyst which suggest us to consider iron phosphide (FeP) as a bifunctional catalyst for electrochemical water splitting.

The second part of this thesis deals with a novel method of synthesizing transition-metal arsenides and the analysis of their properties. Synthesized transition-metal arsenides like FeAs, CoAs, MnAs, and CrAs and their superparamagnetic behavior was investigated. FeAs and CoAs obtained from this synthesis method yielded superparamagnetic nanoparticles with high blocking temperature.

Nanostructured nanomaterials are well known for their changing property as a function of reduced dimension as well as possessing high surface to volume ratio (enhanced surface area). These as-synthesized nanostructures have diverse applications in many fields.

ACKNOWLEDGEMENTS

I would like to start by thanking my advisor, Dr. Manashi Nath, for accepting me into her research group. She had been a constant support and had belief on me which helped in improving myself both academically and as a human being. Her insightful comments and expertise assisted me in building a strong base for understanding my research and nanotechnology. I would like to extend my gratitude to Dr. Xinhua Liang for his constant support and discussions regarding my academic progress. I acknowledge Dr. Sutapa Barua for being one of my committee along with my advisors.

I take this opportunity to express my gratitude to both Chemical Engineering and Chemistry department faculty members and staff for their support and help. I would extend my gratefulness to Materials Research Center for allowing us to use their instruments for doing characterization analysis. I would like to thank my labmates with whom I have been working with till now Jahangir, Wipula, Abdo, Xi, Umanga, Akshay for being with me and guiding me. A special credit to Jahangir for helping me throughout my research and patiently teaching and educating me throughout. I am grateful to my parents and my sister for their unceasing encouragement and for believing in me in my hardships. Also I thank my friends for their constant support and encouragement.

TABLE OF CONTENTS

LIST OF ILLUSTRATIONS

LIST OF TABLES

SECTION

1. INTRODUCTION

Our energy sources are currently dependent on fossil fuels like oil, coal, and natural gas and it is predicted to be depleted in around 100 years. These non-renewable energy resources emit greenhouse gases which creates large environmental problems. The economy, the environment, human health, and increased amount of energy are the primary factors to be considered for renewable and sustainable sources like solar energy, wind energy, geothermal energy, etc. Water electrolysis is an important method to produce hydrogen, which is considered to be another source of clean energy. This is a feasible and the most attractive form of energy source. Renewable fuels generation has emphasized water splitting to produce hydrogen and oxygen and is completely carbon neutral reactions.

1.1 ELECTROCHEMICAL WATER OXIDATION

Electrolysis of water consists of two half reactions which are the hydrogen evolution reaction (HER) and the oxygen evolution reaction (OER). The HER is a less energy demanding reaction when compared with water oxidation (OER), which is considered as the bottleneck in the whole water splitting process. The difficulty of the water oxidation is due to its complexity involving multiple electron transfer process and O-O bond formations [1,2]. Water oxidation is extremely energy demanding and occurs thermodynamically at 1.23V (vs. RHE). The thermodynamics of water splitting is described by following oxygen evolution and hydrogen evolution electrochemical reactions, which can be given as-

At acidic pH:

$$\text{OER:} \quad 2H_2O \rightarrow O_2 + 4H^+ + 4e^- (1.23\text{V vs RHE}) \tag{1}$$

$$\text{HER:} \quad 4H^+ + 4e^- \rightarrow 2H_2 \quad (0.0 \text{ V vs RHE}) \tag{2}$$

And at basic pH:

$$\text{OER:} \; 4OH^- \leftrightarrow 2H_2O + O_2 + 4e^- \; (1.23\text{V vs RHE}) \tag{3}$$

$$\text{HER:} \; 4H_2O + 4e^- \leftrightarrow 2H_2 + 4OH^- \; (0.0 \text{ V vs RHE}) \tag{4}$$
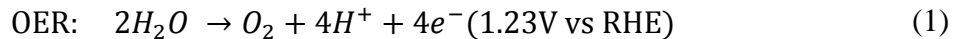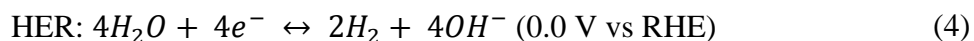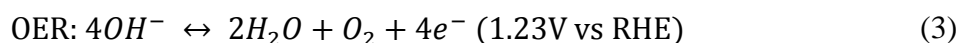
Combining these two equations indicates that a total voltage of 1.23 V is needed to drive the uphill water splitting reaction. An additional voltage is necessary to drive the reaction kinetics or rate of the reaction and the overall voltage for water splitting. In practice, large overpotential is required leading to higher operation potentials. To minimize the overpotential and increase the reaction rate, a catalyst is needed. For large scale applications, the following criteria help in selecting a suitable catalyst for water oxidation, such as long-term durability, low overpotential, high activity, low cost, and low toxicity. The development of effective catalyst for this application is difficult and no catalyst has reached the level of large scale application up to date. The overpotential of the material is from the intrinsic activation barrier occurring at the electrode-solution interface and accounts for resistive losses which can arise from resistance through the electrodes, contacts, or mass transport limitations. While the impact of the overpotential can be minimized through optimal cell designs [3, 4, 5], the activation overpotential is the intrinsic property of the catalysts utilized at the anode and cathode. In real situation, several non-idealities play role for example thermodynamic loss. At redox potential, the reactions are in equilibrium so net reaction rate is zero. A small disturbance from the redox potential is enough to increase either oxidation or reduction but the net production is very less. The

redox potential helps in understanding when the reactions occur but does not explain about the kinetics. The reactions undergo complex steps involving formation/cleavage of chemical bonds or intermediate states. These intermediate products are not stable and need high energy bonding leading to high activation potential, which decelerates the overall reaction. The anode reaction of water splitting is a very complex reaction [6]. One of the O-H bonds must be broken for a proton to be released and two of these O-H intermediates must be present in the close proximity to form O-O bond as shown in Figure 1.1. This is a four electron process and the physical proximity limitation in the anode reaction makes it a complex reaction to occur. This complexity leads to high overpotential requirement resulting in intrinsic loss thus an introduction of catalyst is needed. Hence, an introduction of catalyst is necessary.
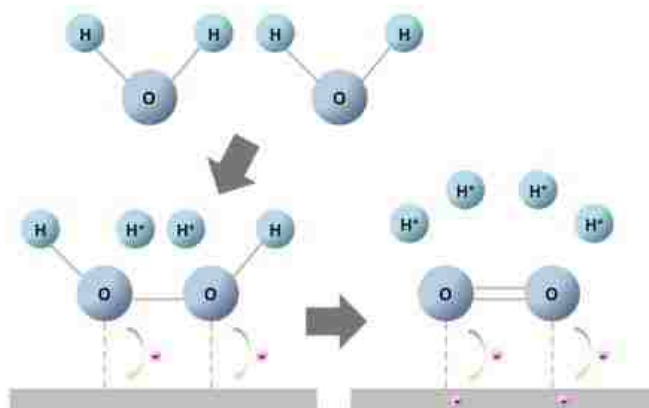
Figure 1.1. Electrochemical water splitting to oxygen molecules

The pH dependency plays a crucial role in understanding the electrochemical reactions. At a given condition, the redox potential does not change and the values depend on the electrochemical environment. The chemical reactions like oxidation and reduction rely on molar concentration corresponding to chemical potential which relates to Nernst equation.

$$E_{red} = E_{red}^o - \frac{RT}{zF}\ln\frac{a_{red}}{a_{ox}} \tag{5}$$

E_{red}: reduction potential

E^o_{red} : standard reduction potential

R : Universal gas constant

T : Temperature

z: valance number

F: Faraday constant

a_{red}: chemical activity of reductant

a_{ox}: chemical activity of oxidant

The slope RT/F at standard condition is 0.0591 V. If a reaction follows a redox potential change of 0.0591 V per log concentration, it follows Nernst equation. In case of water redox reactions, since oxygen and water concentration is assumed constant, the proton concentration is the only variable of reaction potential, which can be expressed by pH as in Figure 1.2., also known as the Pourbaix diagram.

Electrocatalytic systems and their recent research in this field provides us with catalytic motifs as an options. Diverse array of operating conditions includes electrolyte, solvent, working electrode, catalytic activity, efficiency, and stability. Electrochemical references for catalytic operations differ as their use varies greatly depending on the solvent

conditions. A number of problems are still needed to be solved regarding the water oxidation. There are some concerns regarding the catalysts which we choose.
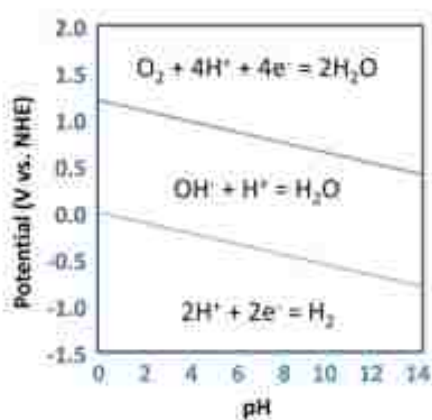
Figure 1.2. Water Pourbaix Diagram

Firstly, durability of the catalyst usually ranges from few minutes to days during the catalytic process. The lifetime of the catalyst for practical purposes needs to be long as it gets decomposed as the reaction proceeds. Secondly, the catalyst should not be air-sensitive otherwise, with the atmospheric oxygen, it will be oxidized rapidly. Ideal water reduction catalyst should be able to initiate hydrogen production at a much faster rate than oxygenation to prevent decomposition or deactivation pathways. Thirdly, working potential for electrocatalytic water splitting is crucial and it should be close enough to the thermodynamic potentials of the two half-reactions for water oxidation and water reduction. For the catalyst if the working potential is too large than an overpotential, then some energy is lost which leads to loss in efficiency. Decreasing the overpotentials to the

minimum levels for water splitting is a challenge in the catalytic process and lots of research is involved in this particular field.

Catalyst helps in building bonds with the dangling bonds of ionic species and transition metals are considered as a preferred catalyst because their electronic configuration can be changed partial occupation of the d-orbital since they have several stable oxidation states. Other factors include lattice distance and crystal direction, which affect their activity.

1.2 EARTH ABUNDANT WATER SPLITTING CATALYSTS

Traditionally catalysts for splitting water are rare earth elements of noble metals like Pt, Ir, and Ru. Even though, these precious metal catalysts show excellent catalytic activity, they are of high cost and low abundance which prevent them from being a potential application for large scale water splitting. Materials based on metal alloys, carbides, sulfides, and phosphides show high activity of HER and cobalt phosphate, metal oxides, and hydroxides demonstrate good activity for OER[7]. Research in this area shows very few earth abundant catalysts are capable of catalyzing both HER and OER in the same pH range for full water splitting. But recent research has discovered that transition-metal phosphides can be used for this purpose effectively.

1.2.1 Metal Phosphides. Main-group metal phosphides are formed with phosphide anions, P3- and a less electronegative metal. These compounds include Na_3P, Ca_3P_2, GaP, InP, Cu_3P, Cu_3P_2, etc. GaP [8] and InP [9] are semiconductors at room temperature and are used in making LEDs as their band gaps are accurate and can be doped in the semiconductor lattice. This band gap helps in tuning the emission and electronic properties

of the metal phosphides. For instances, GaP nanowires give high efficiency green light [10] and InP is a good solar cell material. The most common synthesis method for making metal phosphides is using precursors like trioctylphosphine (TOP) and tricoctylphosphine oxide (TOPO) [11]. Many research results convince that phosphides are functional materials. They display extraordinary applications and their synthesis method is simple and reproducible.

1.2.2 Nanostructured Transition-metal Phosphides. The property change in nanostructured phosphides is attributed to the reduced dimensions and the intrinsic property of the material. When these materials are nanostructured, the properties related to electrons and their mobility are altered or enhanced accordingly. Nanostructured transition metal phosphides are investigated by various groups. Dodecylamine-capped FeP nanoparticles show magnetic moments within each particle as antiferromagnetic in contrast with bulk FeP and no Neel relaxation was observed [12]. Synthesis of FeP, Fe_2P, MnP, MnAs and Ni_2P nanoparticles by precipitation method has been reported giving narrow size distribution of nanoparticles [13, 14, 15]. When Fe nanoparticles gets converted to FeP and Fe_2P nanorods they show ferromagnetic behavior with a transition temperature of 179 K, whereas bulk FeP was metamagnet with a Neel temperature of 120K [13].

1.3 RESEARCH PROBLEM

In the past, transition-metal chalcogenides, nitrides, and carbides have shown excellent electrocatalytic acitivity [16]. Recently, transition-metal phosphides (TMP) open a new research stream as electrocatalyst towards water splitting. They gain interest as they are very active towards HER in electrolytes of all pH range [16]. Iron phosphide displays

chemical and physical properties similar to nitrides and carbides. This metal-rich TMP is also a good conductor of heat and electricity and has high thermal and chemical stability [16]. Further, in contrast to transition-metal chalcogenides FeP does not form layered structures which has an advantage of better active sites on the crystal surface. This makes FeP beneficial for electrocatalytic material for both OER also. Many research is going on for a potential bifunctional catalyst for electrochemical water splitting and FeP is one amongst them and in this work, FeP as a bifunctional catalyst for overall water splitting is developed.

1.4 CATALYTIC ACTIVITY OF FeP

1.4.1 Hydrogen Evolution Reactions. Extensive study about potential pathway for proton reduction is very important for effective hydrogen evolution catalyst. Hydrogen evolution usually proceeds through a metal hydride intermediate which is formed either by consecutive or coupled proton and electron transfers. The metal-hydride should have open active sites and appropriate electronic characteristics for hydrogen production.

For hydrogen evolution, at the interface between the solid catalyst and the electrolyte, solvated protons from the liquid gain electrons from the electrode. These are the reactions which are believed to be undergoing and * denoted the catalytic active site.

$$HA + * \rightarrow H^* + A^- \tag{6}$$

$$H^* + HA \rightarrow H_2 + A^- \tag{7}$$

$$2H^* \rightarrow H_2 \tag{8}$$

There are two possible mechanisms invoked for hydrogen evolution. The solvated protons from the electrolyte start to absorb on the catalyst surface which combines with the

electrons. This reaction is called Volmer step. The two adsorbed H atoms on the surface of the catalyst may combine to give H_2 molecule. This reaction is known as Tafel step. Alternately, a solvated proton may directly react with a hydrogen atom and an electron on the surface and form an H_2 molecule. This reaction is familiarly known as the Heyrovsky step. The second proton never binds on the surface of the catalyst. For the overall reaction to occur it should either happen through Volmer-Tafel mechanism or Volmer-Heyrovsky mechanism.

Au-coated glass substrates were used in preparing the electrode for studying both Oxygen evolution and Hydrogen evolution reactions. All solutions were prepared using deionized (DI) water . Prior to electrodeposition, the substrates were cleaned by ultrasonic treatment followed by isopropanol rinse for three times and eventually rinsed with deionized water (15 min each step) to ensure the clean surface. FeP catalyst ink was prepared by ultrasonically dispersing 10.0 mg catalysts in 1.0 mL isopropyl alcohol (IPA) and ultrasonicated for 30 min. Au-coated glass plates was covered with a Teflon tape, leaving an exposed geometric area of 0.283 cm^2, served as an underlying conductive substrate of the working electrode. A quantity of 20 μL of the ink was pipetted out on the top of the Au. The catalyst layer was dried at room temperature. Then, an aliquot of Nafion solution (10 μL of 1 mg/mL solution in 50% IPA in water) was applied onto the catalyst layer. The Nafion-coated working electrode was dried at room temperature and finally heated at 130 ºC for 30 min in air in an oven.

The electrocatalytic activity for catalytic HER with FeP over Au-coated glass was determined in N_2-saturated 1.0 M KOH , 0.5M H_2SO_4, and 1.0 M PBS solutions at a scan rate of 10 mV s^{-1}.

1.4.1.1 Hydrogen evolution reaction in alkaline medium. From the Figure 1.3., HER activity is exhibited clearly with an onset potential of 220 mV and an overpotential of 390 mV to achieve 10 mA cm^{-2}. The observed tafel plot show 157 mV per decade.
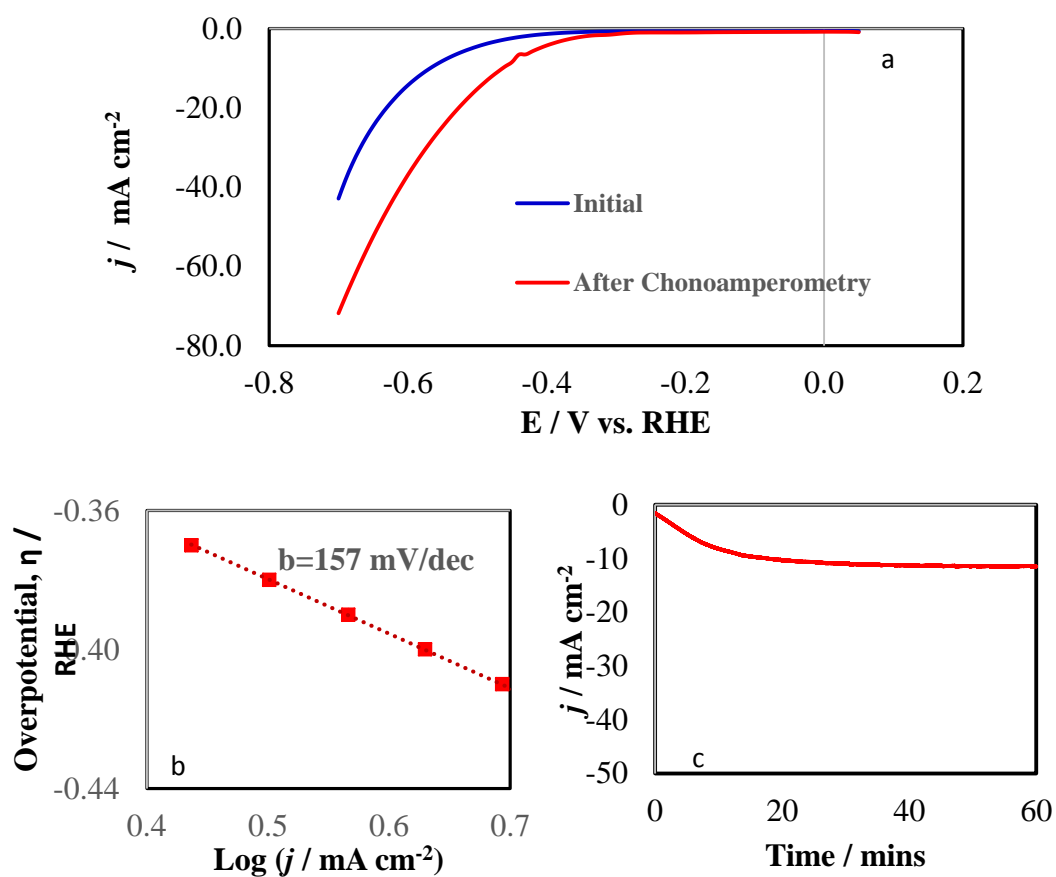
Figure 1.3. (a) LSV for HER in 1.0 M KOH at a scan rate of 10mV s^{-1} (b) Tafel plot of catalyst (c) stability for 1 hr of the catalyst

1.4.1.2 Hydrogen evolution reaction in acidic medium. From the figure 1.4., HER activity is exhibited clearly with an onset potential of 100 mV and an overpotential of 317 mV to achieve 10 mAcm^{-2}. A stability study was conducted and Figure- (b) shows that the catalyst is stable under H$_2$ evolution for one hour. The observed tafel plot show 95.6 mV per decade.

Figure 1.4. (a) LSV for HER in 0.5 M H$_2$SO$_4$ at a scan rate of 10mV s^{-1} (b) Stability study for 1 hr of the catalyst (c) Tafel plot of catalyst

1.4.1.3 Hydrogen evolution reaction in pbs medium. From the Figure 1.5.,

HER activity is exhibited clearly with an onset potential of 115 mV and an overpotential

of 275 mV to achieve 10 mA cm^{-2}. A stability study was conducted and figure -(b) shows

that the catalyst is stable under H$_2$ evolution for one hour. The observed tafel plot show
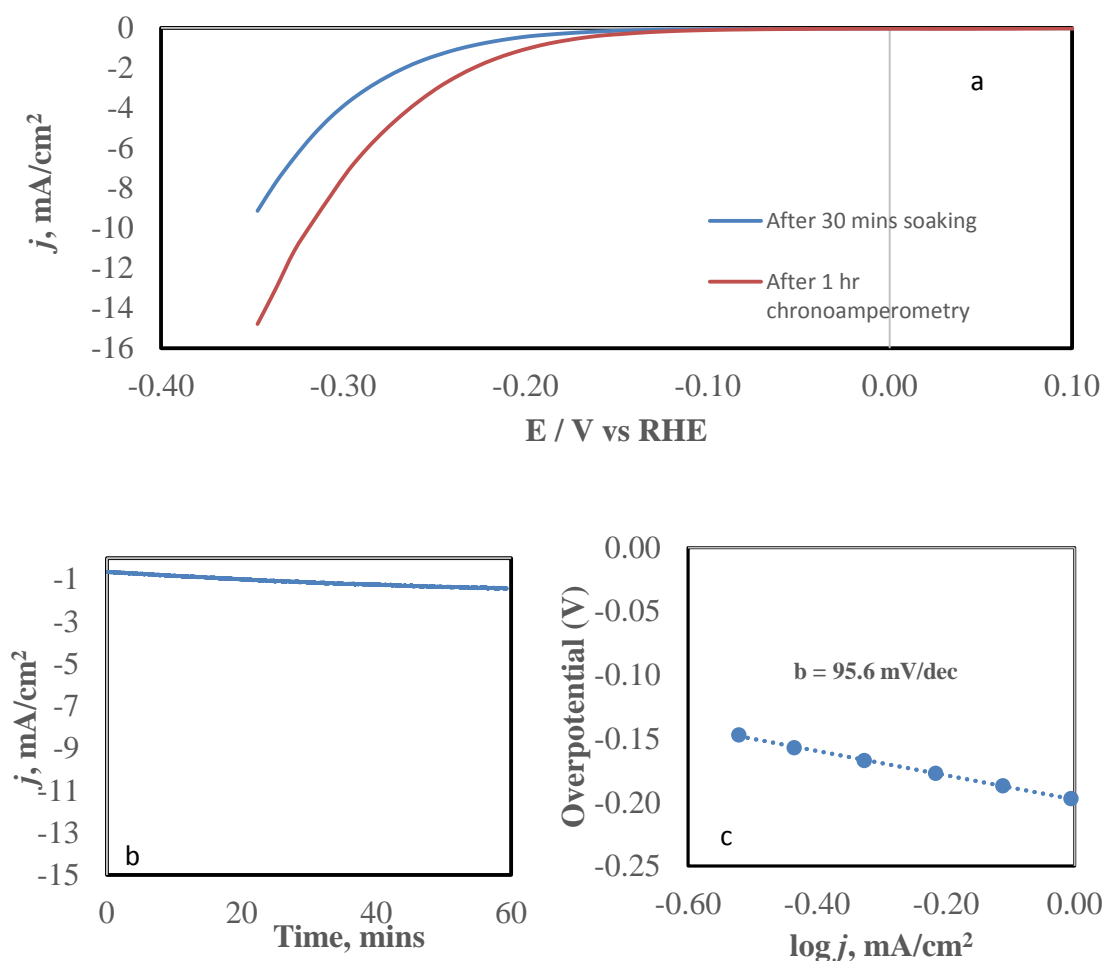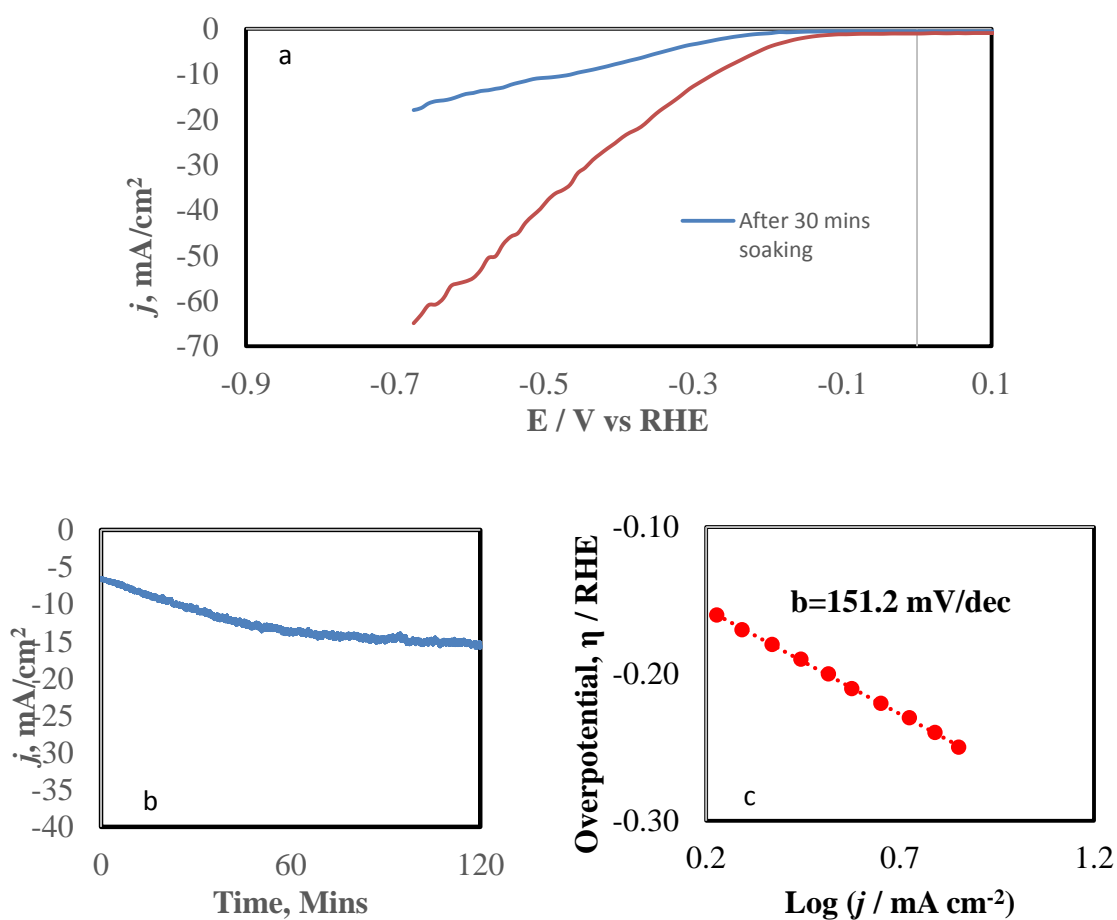
151.23 mV per decade.

Figure 1.5. (a) LSV for HER in 1 M PBS at a scan rate of 10mV s^{-1} (b) Stability study for
1 hr of the catalyst (c) Tafel plot of catalyst.

1.4.2 Oxygen Evolution Reactions. Oxygen evolution reaction (OER) is a common and an important anodic process in electrolysis process in aqueous medium. Numerous metals and alloys have been approved to be electrocatalyst and among them nickel and noble metals are the best option. Industrial electrochemical process like water electrolysis prefer a stable anode material with low overvoltage. The main prerequisites for the anode material for OER production are high surface area, high electrical conduction, good electrocatalytic behavior, minimization of gas bubble problems, low cost and safety with respect to health. These characters influence the electrode reaction and the overpotential of the catalyst in OER. The comparison of the overpotential at a constant current density or the current density at a constant overpotential is a more advantageous way for elucidating electrocatalysis for pragmatic use. The OER mechanism is complex when compared to HER because many intermediate states exist in the reaction steps and at times there might be many activation steps which controls the rate of the OER. The active site of a transition metal is on the surface, will involve in decreasing the activation energy in the rate controlling step also contributes to the electron transfer. The main factors which determine the electrocatalysis for OER are the bond strength between the transition metal and the oxygen atom because it affects the rate of desorption and the adsorption steps. The other factor is due to the electron transfer rate which relates the density of the electron states at the fermi level and the degree of overlapping between the orbitals of the active site. The adsorbed species at the electrode surface will help in determining the rate of the electron transfer.

PAPER

I.   **EARTH ABUNDANCE METAL PHOSPHIDE (IRON PHOSPHIDE) AS AN EFFICIENT CATALYST FOR OXYGEN EVOLUTION REACTIONS IN ALKALINE SOLUTION**

N. Ashokan,[a] J. Masud[b] and M. Nath[b],*

[a]Department of Chemical and Biological Engineering, Missouri University of Science & Technology, Rolla, MO 65409.

[b]Department of Chemistry, Missouri University of Science & Technology, Rolla, MO 65409.

Email: nathm@mst.edu

ABSTRACT

Herein, for the first time, we report solution phase synthesis of iron phosphide as efficient catalyst for oxygen evolution reaction. It needs only 290 mV overpotential to achieve a current density of 10 mA cm^{-2} with small Tafel slope of 50.8 mV/decade and maintains high stability in 1 M KOH.

1. INTRODUCTION

The development of renewable and clean energy technologies, [1-3] such as water splitting for hydrogen production, artificial photosynthesis and metal-air batteries, is hindered because of very sluggish oxygen evolution reaction (OER) kinetics. Despite Ru, Ir based catalysts being known as highly effective OER catalysts, [4-5] their prohibitive cost and scarce reserves have significantly prohibited large-scale application. Therefore, it is highly desirable and imperative to develop new OER electrocatlysts with both excellent activity and low cost. Consequently, great efforts have been devoted to developing low-cost alternatives. Recently, transition metal oxides [6-7] have been subject of intense research as an alternative electrode materials of these expensive noble metals. Beside oxides, transition metal chalcogenides [8-9], nowadays, considered as potential candidate for the OER due to their remarkable electronic structures [10]. More recently, transition-metal phosphides (TMPs) [11-18] which are intrinsically metallic have been intensively studied as an electrocatalysts for OER and HER. For instance, FeP [11], Ni_2P [12], CoP [13], etc. have already shown great potentials as HER catalysis at high current densities and at low overpotentials. On the other hand, there have been few reports on TMPs (e.g., CoP, NiP) as OER catalyst in alkaline media. Recently, Yan et. Al [18] has reported iron phosphide nanotubes coated with an iron oxide/phosphides @ carbon cloths as full water splitting catalyst. Herein, we report that solution phase synthesis of iron phosphide (FeP) can be directly utilized as electrocatalysts for OER in strong alkaline electrolyte, which can achieve a current density of 10 mA cm^{-2} at overpotentials of 290 mV for OER with very small Tafel slopes, 50.8 mV/dec. Electrode prepared from FeP catalyst shows an excellent stability and activity after 4 h of constant current electrolysis.

2. CHARACTERIZATION OF FeP

Figure 1.1. (a) shows the TEM image and corresponding histogram (inset of Figure. 1.1. (a) where catalyst was found to be uniform particles size with a narrow size distribution (from 3-7 nm), centered at 5 nm based on the counting of 100 randomly chosen particles. The high-resolution TEM (HRTEM) image, as shown in Figure. 1.1. (b), reveals the lattice fringes with interplanar spacings of 1.54, 2.42 and 2.73 Å, corresponding to <020>, <111> and <011> planes of the FeP, respectively. The crystallinity of film was further confirmed by SAED pattern shown as inset of Figure 1.1 (b) where bright rings made up of discrete spots, which can be indexed to the <111> and <211> planes of FeP, respectively. The TEM EDS spectrum of FeP imples the presence of Fe and P elements with the atomic ratio close to 1:1. Pxrd was carried out to further characterize the chemical structures of the as-prepared catalyst. As shown in Figure 1.1. (c), all the diffraction peaks could be well indexed to FeP (JCPDS Card No.01-078-1443), with almost no detectable impurities. The X-ray photoelectron spectroscopy (XPS) analysis of the as-prepared FeP is shown in Figure 1.1 d. The doublet peaks for the binding energy (BE) of Fe 2p3/2 appear at 707.1 and 711.8 eV and P 2p peaks at 129.3 and 133.8 eV. The peak at 707.1 eV is associated with Fe in FeP,[19] hereas that of 711.8 eV due to oxidized Fe,[20] resulting from the superficial oxidation of FeP exposed to air.[20] The P 2p XPS spectrum reveals two peaks at 133.6 and 129.4 eV, respectively. The lower energy peak is consistent with the binding energy for FeP (129.4 eV),[19,20] and peak at 133.6 might due to the presence of oxidized phosphorus as the samples were exposed to air.

Figure 1.2. shows the polarization curves of FeP @ Au and bare Au in N_2 saturated 1 M KOH at a scan rate of 10 mV s^{-1}. Bare Au clearly did not have catalytic activity (or

very poor activity). But the loading of FeP on Au showed excellent onset potential and overpotential for OER. Specifically, the onset potential of FeP @ Au was 1.48 V (vs. RHE) and yielded a current density of 10 mA cm^{-2} at an overpotential of 320 mV, which was comparable to IrO_x (320 mV) [21] and /-or better than the metal phosphide based catalysts. At this stage it is difficult to explain the reason of enhanced OER activity at FeP. One of the reasons might due to the high electrical conductivity of FeP like other transition metal phosphides [14], which may favors fast electron transport and enhances the activity. Inset of Figure 1.2. presents Tafel plot, η vs. log(j), for FeP @ Au. The Tafel slope, 50.8 mV/dec is comparable for all TMPs based OER [15-17].

The stability of catalyst was performed through the time dependent voltages under a constant current of 10 mA cm-2 for 4h and shown in Figure 1.3. Initially the high overpotential was required to achieve 10 mA cm^{-2} compare to after 4h. The inset of Figure 1.3. depicts comparison of LSVs showed the better activity after 4 h of chronopotentiometry (only 290 mV overpotential requires to get 10 mA cm^{-2}) compared to the initial curve, suggesting the superior stability of catalyst in the long term process. The SEM implies the electrode surface remained unchanged after 4 h of continuous electrolysis and EDX line scan shows the uniform distribution of Fe and P in both of before and after activity catalyst film.

The turnover frequency (TOF) of the FeP catalyst was calculated at an overpotential of 370 mV in 1 M KOH, assuming all of the active metals in the catalyst are catalytically active for OER. The TOF value of FeP were calculated to be 0.021 and 0.032 s^{-1} for initial and after 4 h of chronopotentiometry, respectively which are comparable with the previously reported TOF values of metal phosphide based catalyst[17] , and higher than

well-known IrO$_x$ (0.0089 s^{-1}) [22] OER catalyst, also indicating a better OER activity on FeP. This enhanced activity after 4 h of choropotentiometry compare to the initial might be due to the increasing of wettability of the thin Nafion layer covering the catalysts particles with time, which may allow the electrolyte to the contact of active material surfaces. Table 1.1. Compares different OER catalysts.
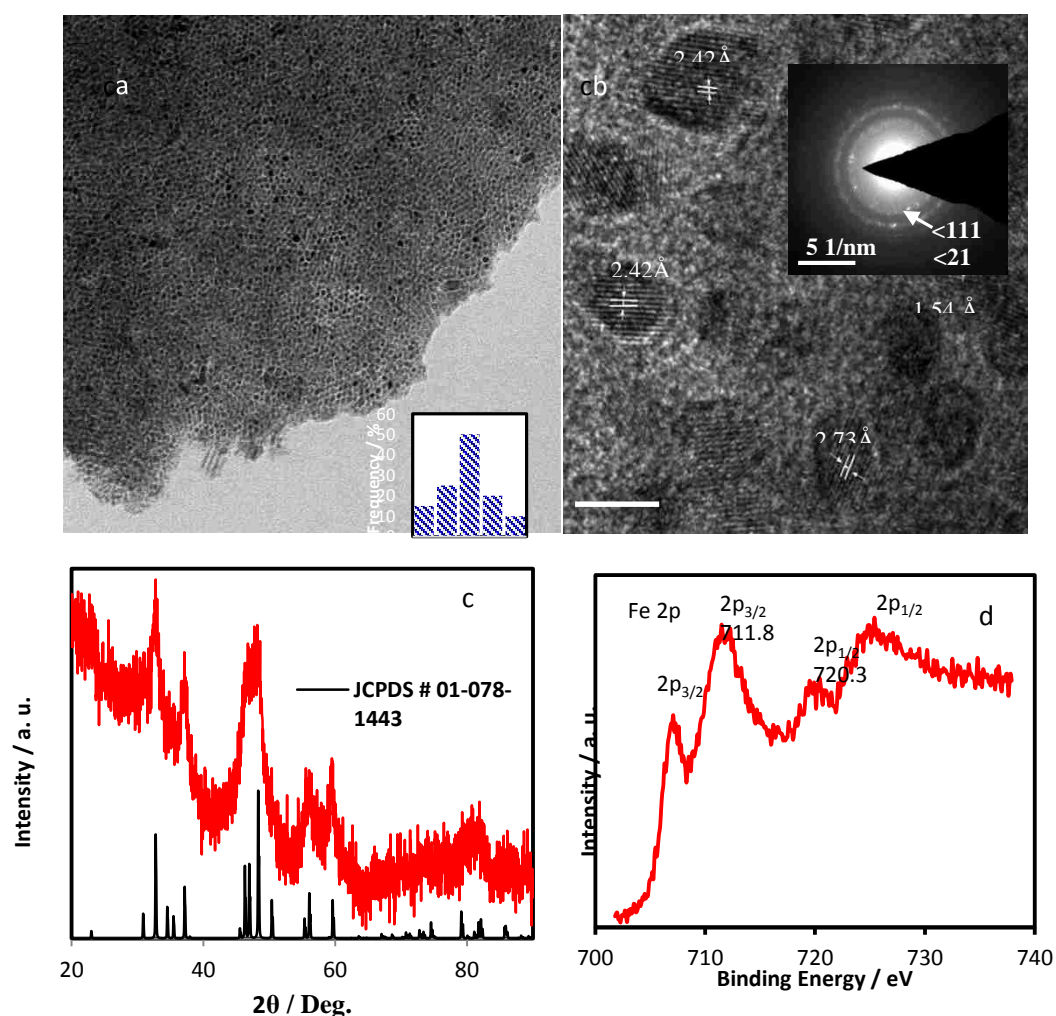

Figure 1.1. (a) TEM images of FeP and particle size histogram (inset), (b) HRTEM image and corresponding selected-area electron diffraction (SAED) pattern, (c) Pxrd of FeP, and (d) XPS spectra of Fe 2p and P 2p (inset)
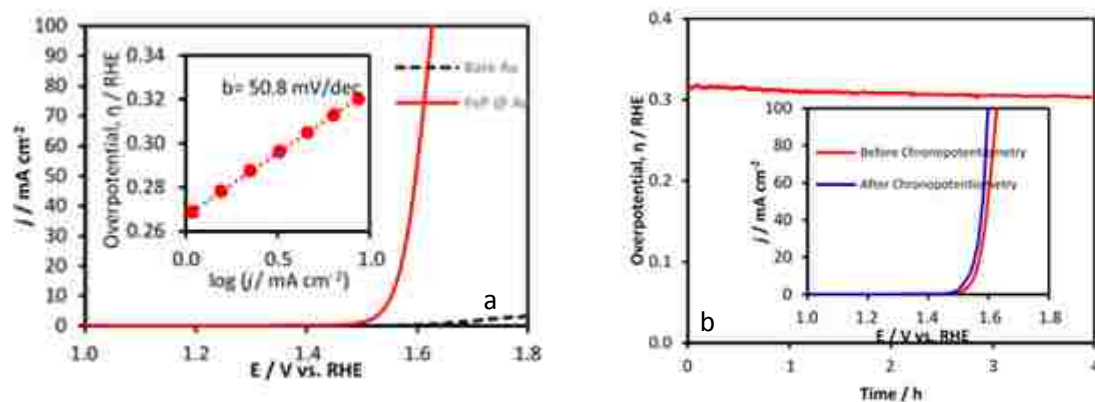
Figure 1.2. (a) LSVs measured in N_2 saturated 1.0 M KOH solution at a scan rate of 10 mV s^{-1} and inset is the Tafel plot of catalyst, (b) Stability study of catalyst under continuous O_2 evolution (at 10 mA/cm^2) for 4 h studied through chronopotentiometry. Inset shows the LSVs of catalyst synthesized in N_2 saturated 1 M KOH before and after chronopotentiometry for 4 h.

Table 1.1. Comparison of OER activity at different catalysts.

Catalyst	Electrolyte	Onset potential / vs. RHE	η at 10 mA cm^{-2} / mV	Tafel / mV dec^{-1}	TOF at 370 mV / s^{-1}	References
$(Co_{0.54}Fe_{0.46})_2P$	0.1 M KOH	1.46	370	-	-	14
Ni-P	1.0 M KOH	1.54	344	49	-	15
CoP	1.0 M KOH	1.56	345	47	-	16
CoP NPs	0.1 M NaOH	1.52	330	50	0.0287	17
Iron Oxide/phosphate layer coated FeP	1.0 M KOH	1.48	288	43	-	18
FeP	1.0 M KOH	1.48	Initially 320 After 4h 290	51	0.021 0.032	This work

3. CONCLUSION

In summary, we reported a simple synthesis of the topmost earth-abundant metal phosphide based, FeP, catalyst for the oxygen evolution reaction in alkaline solution. This catalyst requires comparatively lower overpotential to achieve the 10 mA cm^{-2} which is, even, lower than the overpotential of robust IrO$_x$ catalyst. FeP is reported as the OER catalyst for the first time which requires comparatively lower overpotential (290 mV) to achieve the 10 mA cm^{-2} and exhibited a very high stability in alkaline media.

APPENDIX

SYNTHESIS OF FeP

All reagents used in this synthesis were purchased from Sigma Aldrich. In a typical experiment, 1.00 g of trioctylphosphine oxide (TOPO) and 1.2 ml of trioctylphosphine (TOP) were mixed and heated at 300°C for 30 mins in a three neck round bottom flask under vigorous stirring in N_2 medium. Subsequently, 0.3 mL of solution 1 (made from 0.2 mL of $Fe(CO)_5$ and 0.8 mL TOP) were added into the TOP/TOPO solution. Instantly, the solution changed to black and the temperature was constantly maintained at 300°C for 30 mins. The black solution was washed and centrifuged several times with hexane using ultrasonification to remove the unreacted reactants. The black product was dried and characterized.

ELECTRODE PREPARATION

Au-coated glass substrates were purchased from Deposition Research Lab Incorporated (DRLI), Lebanon Missouri. All solutions were prepared using deionized (DI) water with a resistivity of 18 MΩ·cm. Prior to electrodeposition, the substrates were cleaned by ultrasonic treatment in micro-90 followed by isopropanol rinse for three times and eventually rinsed with deionized water (15 min each step) to ensure the clean surface. FeP catalyst ink was prepared by ultrasonically dispersing 10.0 mg catalysts in 1.0 mL isopropyl alcohol (IPA) and ultrasonicated for 30 min. Au-coated glass plates was covered with a Teflon tape, leaving an exposed geometric area of 0.283 cm^2, served as an underlying conductive substrate of the working electrode. A quantity of 20 μL of the ink was pipetted out on the top of the Au. The catalyst layer was dried at room temperature.

Then, an aliquot of Nafion solution (10 μL of 1 mg/mL solution in 50% IPA in water) was applied onto the catalyst layer. The Nafion-coated working electrode was dried at room temperature and finally heated at 130 °C for 30 min in air in an oven.

CHARACTERIZATIONS AND CATALYTIC ACTIVITY

Characterizations: Transmission Electron Microscopy (TEM): FEI Tecnai F20 was used to obtain TEM, high resolution TEM images (HRTEM) and selected area electron diffraction (SAED) patterns of the catalysts.

Powder X-ray Diffraction. The electrodeposited substrates were studied as such without any further treatment. The product was characterized through powder X-ray diffraction (pxrd) with Philips X-Pert using CuKα (1.5418Å) radiation. Pxrd pattern was collected from the as-synthesized product spread on the growth substrate. Because the product formed a very thin layer on the substrate, the pxrd was collected at grazing angles in thin film geometry (GI mode with Göbel mirrors).

X-ray Photoelectron Spectroscopy (XPS): XPS measurements of the catalysts were performed by KRATOS AXIS 165 X-ray Photoelectron Spectrometer using monochromatic Al X-ray source. The spectra were collected for the as-prepared sample and the sample after sputtering with Ar for 2 min, which removed approximately 2 nm from the surface.

ELECTROCHEMICAL CHARACTERIZATION AND CATALYTIC STUDIES

The OER catalytic performance was estimated from linear scan voltammetry (LSV) plots while the stability of the catalyst was studied by chronoamperometry.

Electrochemical measurements were performed in a three-electrode system with an IvumStat potentiostat using Ag/AgCl and Pt mesh as reference and counter electrodes, respectively. All measured potentials vs the Ag/AgCl were converted to the reversible hydrogen electrode (RHE) scale via Nernst equation (eq. 1):

$$E_{RHE} = EAg/AgCl + 0.059 \text{ pH} + E_oAg/AgCl \tag{1}$$

where E_{RHE} is the converted potential vs. RHE, EAg/AgCl is the experimentally measured potential against Ag/AgCl reference electrode, and $E_oAg/AgCl$ is the standard potential of Ag/AgCl at 25 °C (0.197 V). For most of the electrochemical characterizations, the electrode area of the film surface was kept constant at 0.283 cm^2.

Turnover Frequency (TOF). The turnover frequency (TOF) was calculated from the following equation:

$$TOF = I/(4 \times F \times m) \tag{2}$$

Where I is the current in Amperes, F is the Faraday constant and m is number of moles of the active catalyst.

Tafel plots. The Tafel slope was calculated from the following equation:

$$\eta = a + (2.3 \text{ RT})/\alpha nF \log(j) \tag{1}$$

where η is the overpotential, j is the current density and the other symbols have their usual meanings.

The Tafel equation as shown in Eq. (1) is a fundamental equation which acquires from the kinetically controlled region of OER / HER, and relates the overpotential η with the current density j where the Tafel slope is given by 2.3RT/αnF. To calculate Tafel slopes, LSV plots were obtained with a slow scan speed (2 mV s^{-1}) in non-stirred solution.

REFERENCES

1.   M. G. Walter, E. L. Warren, J. R. McKone, S. W. Boettcher, Q. Mi, E. A. Santori and N. S. Lewis, Chem. Rev. 2010, 110, 6446.

2.   J. R. Mckone, N. S. Lewis and H. B. Gray, Chem. Mater. 2014, 26, 407.

3.   N. S. Lewis and D. G. Nocera, Proc. Natl. Acad. Sci. U. S. A. 2006, 103, 15729.

4.   Y. Lee, J. Suntivich, K. J. May, E. E. Perry and Y. Shao-Horn, J. Phys. Chem. Lett., 2012, 3, 399.

5.   J. Jiang, A. Zhang, L. Li and L. Ai, J. of Power Sources, 2015, 278, 445.

6.   W. T. Hong, M. Risch, K. A. Stoerzinger, A. Grimaud, J. Suntivich and Y. Shao-Horn, Energy Environ. Sci. 2015, 8, 1404.

7.   F. Jiao and H. Frei, Angew. Chem., Int. Ed. 2009, 48, 1841.

8.   A. Swesi, J. Masud and M. Nath, Energy Environ. Sci., 2016, DOI: 10.1039/C5EE02463C.

9.   Y. R. Zheng, M. R. Gao, Q. Gao, H. H. Li, J. Xu, Z. Y. Xu and S. H. Yu, Small, 2015,11, 182.

10.   Y. Liu, H. Cheng, M. Lyu, S. Fan, Q. Liu, W. Zhang, Y. Zhi, C. Wang, C. Xiao, S. Wei, B. Ye and Y. Xie, J. Am. Chem. Soc., 2014, 136, 15670.

11.   Z. Zhang, B. Lu, J. Hao, W. Yang and J. Tang, Chem. Commun., 2014, 50, 11554.

12.   E. J. Popczun, J. R. McKone, C. G. Read, A. J. Biacchi, A. M. Wiltrout, N. S. Lewis and R. E. Schaak, J. Am. Chem. Soc., 2013, 135, 9267.

13.   F. H. Saadi, A. I. Carim, E. Verlage, J. C. Hemminger, N. S. Lewis and M. P. Soriaga,J. Phys. Chem. C, 2014, 118 , 29294.

14.   A. Mendoza-Garcia, H. Zhu, Y. Yu, Q. Li, L. Zhou, D. Su, M. J. Kramer and S. Sun,Angew. Chem. Int. Ed. 2015, 54, 9642.

15.   N. Jiang,. B. You, M. Sheng and Y. Sun, ChemCatChem, 2015, DOI:10.1002/cctc.201501150.

16. N. Jiang,. B. You, M. Sheng and Y. Sun, Angew. Chem. Int. Ed., 2015, 54, 6251.

17. C. C. Hou, S. Cao, W. F. Fu and Y. Chen, ACS Appl. Mater. Interface, 2015, DOI: 10.1021/acsami.5b09207.

18. Y. Yan, Y. X. Bao, X. Ge, Z. Liu, Chem. Eur. J. 2015, 21, 18062.

19. H. Du, S. Gu, R. Liu and C. M. Li, Int. J. of Hydro. energy, 2015, 40, 14272.

20. J. Tian, Q. Liu, Y. Liang, Z. Xing, A. M. Asiri and X. Sun, ACS Appl. Mater. Interfaces, 2014, 6, 20579.

21. C. C. L. McCrory, S. Jung, J. C. Peters and T. F. Jaramillo, J. Am. Chem. Soc. 2013,135, 16977.

22. L. Trotochaud, J. K. Ranney, K. N. Williams and S. W. Boettcher, J. Am. Chem. Soc. 2012, 134, 17253.

SECTION

2. CONCLUSIONS AND FUTURE WORK

The topmost earth-abundant metal phosphide, FeP, catalyst for the oxygen evolution reaction in alkaline solution shows comparatively lower overpotential to achieve the 10 mA cm^{-2}. In this thesis, FeP obtained has a lower overpotential of 290 mV to achieve the 10 mA cm^{-2} and exhibited very high stability in alkaline media. FeP catalyst for Hydrogen Evolution Reaction in alkaline, acidic and neutral solution shows overpotential of 470 mV, 317mV, and 275 mV respectively. Future steps can involve in checking the catalytic activity of FeP for Oxygen Reduction Reactions (ORR) making it a trifunctional catalyst. FeP nanorods and nanostructure arrays would provide better catalytic activities.

APPENDIX

INTRODUCTION

Main-group metal phosphides are formed with anions, P^{3-} and a less electronegative metal. GaAs is a direct band-gap semiconductor. When it is combined with zinc blende its characters as semiconductor improves as its electron mobility increases. This is a good material for making high frequency transistors. GaAs nanoparticles especially quantum dots based have good electronic and optical properties [16]. Metal arsenides have their importance as detectors, photodiodes and solar cells.

TRANSITION-METAL ARSENIDES

Both transition arsenides and phosphides come under the category of transition-metal pnictides and they are gaining importance due to their d-electron configuration of the central atom. Fe-based pnictides show superconductivity property [18] which can store charge layers. Binary EAs are formed when transition metals in +3 oxidation state combines with -3 oxidation state of As. Binary arsenides are of mostly with transition metals which have partially filled 3d shell which is highlighted in the Figure A1.

Many other transition-metal pnictides are RhP_3, RuP, Ru_2P, Pd_3P, Ni_2P, MoP, FeP,etc. These transition-metal pnictides have their applications in electronic, magnetic properties and electrochemical properties also due to their facile redox chemistry. Magnetic properties of these transition-metal pnictides are rare and they can be implemented in magnetic refrigeration built on magnetocaloric effect (MCE). If a material exhibits MCE, when an external magnetic field is applied the magnetic moment gets oriented randomly

giving heat. This heat can be extracted from the MCE material through heat transfer and given out to the atmosphere. If the magnetic field is taken off, magnetic moments get randomized again, cooling the environment below the ambient temperature because of the heat withdrawal from the material. $MnFeP_{0.45}As_{0.55}$ is an example of MCE at room temperature [19,20].

Figure A1: Binary Arsenides formed from transition metals

Transition-metal pnictides have their importance in superconductivity after the discovery of Fe based pnictides, especially arsenides because they exhibit high T_c (critical temperature for superconductivity). Even Fe-based phosphides display superconductivity, one such material is $La_{0.8}Rh_4P_{12}$ with a T_c of 13.6 K [21]. To conclude, transition-metal arsenides and phosphides have their usefulness in superconductivity and magnetism [22,23].

NANO-STRUCTURED METAL ARSENIDES

Magnetism and superconductivity are expected to display unique features when they are nanostructures. Reduction in dimension of superconductors develops artificial potential wells where the superconducting flux lines are confined and the boundary conditions of the potential wells change leading to change in properties similar to quantum confinement known as quantum size effect in superconductors. Nano-magnetism is a scope of research in magnetic phenomenon occurring at submicron level. Binary transition-metal pnictides especially arsenides when nanostructured show interesting magnetic interactions. In ferromagnetic materials, when the material size is reduced below to critical size the magnetic spins get confined in a single magnetic domain. This effect makes the particle to behave as monodomain magnetic chunks thereby to superparamagnetic behavior. Nanostructuring breaks the electron pair and makes the surface magnetic phenomenon more prominent causing ferromagnets and antiferromagnets to exhibit unique properties.

SYNTHESIS METHOD OF TRANSITION-METAL PNICTIDE

Nanomaterial synthesis using novel, facile and scalable methods provides way to new evolution of materials with varied applications. Many advancement, improvements and establishments have been made in the synthesis methods of nanomaterials in the past few decades. Some common synthesis methods are being illustrated. Cobalt phosphide (Co_2P) nanowires were synthesized using one pot synthesis with cobalt oleate in TOP at 290˚C or 320˚C [24]. Co_2P or CoP nanoparticles of 5nm were achieved using cobalt diselenophosphinate precursor dissolved in TOP to TOPO or HDA at 300˚C after 60 and 150 mins respectively. Thermolysis of $Co(C_5H_7O_2)_2$ precursor in TOPO at 350˚C for 5h

gives Co_2P [25]. General method of converting metal nanoparticles to transition-metal phosphides such as Ni_2P, PtP_2, Rh_2P, PdP_2, Pd_5P_2, and Au_2P_3 is by reacting TOP in a hot solvent at 360˚C. In this method, metal nanoparticles act as reactive template to produce these transition-metal phosphides [26,27]. TOP can be used as an applicable precursor in the synthesis of metal phosphides from metal nanoparticles. Fe phosphide nanoparticles can be synthesized through reductive annealing of Fe phosphate nanoparticle as a precursor casted on mica surface [28]. This route can be applied for a wide range of transition metals and pnictogens to avoid highly toxic precursors for synthesis. FeP nanoparticles can be also synthesized using Fe(III) acetylacetonate with tris(trimethylsilyl)phosphine at 320˚C with TOPO as a solvent and decylamine, myristic acid or hexylphosphonic acid as capping agents [13]. FeAs nanocrystals were made by reductive recombination reaction with transition metal chrolides like $FeCl_3$ and $AsCl_3$ at 150-180˚C [29]. This synthesis method did not give an insight about the magnetic nature and the morphology was also unclear. The synthesis method of arsenside nanostructures through solution chemistry has Sa-precursor like $AsCl_3$, AsH_3, and As, which are toxic. Lately, triphenylarsenide (TPA) is being used as an alternative As-precursor in the synthesis of InAs and GaAs [30]. TPA is less toxic, easy to handle, and moderately reactive, which makes it a preferred candidate as As-precursor for synthesizing arsenide nanostructures. Mesh like CoAs nanostructures [31] and thin film CoAs using metal-organic complex 1,3-bis(tert-butyl)-2-112[tetracarbonyl-cobalt(-1)]-1,3,2-diazarsolidine were synthesized using chemical vapor deposition method [32]. These conventional methods produce pure sample, but their morphology cannot be controlled.

SYNTHESIS OF BINARY METAL ARSENIDES

A general method for synthesis of EAs nanoparticles was carried out in a nitrogen filled glove box containing less than 1 ppm of O_2. The experiment was carried out in a three-neck round bottom flask assembled with a magnetic stirring bar and air condenser. To this round bottom flask 1mM of triphenylarsine (TPA) and 5 mM of HAD was weighed and added. This mixture was heated to 325˚C and the reactants melt to form a colorless solution. 1mM of $Fe(CO)_5$,/$Co_2(CO)_8$,/$Mn(CO)_5$,/$Cr(CO)_6$ was then injected using a syringe or as solid into the hot HDA + TPA mixture. After the addition of the carbonyl precursor the solution turns black immediately with rapid evolution of gases. After the gas subsides, the black solution gets refluxed depending on the reaction for variable length of time and the heating is stopped and allowed to cool down to room temperature. The black solution was washed 3-4 times with ethanol and hexane using ultra-sonication to remove excess HDA or any other unreacted precursors. The powder gets settled at the end of the centrifuge tube which is air dried and collected for further characterization. The powder was characterized using powder X-ray diffraction (pxrd), scanning and transmission electron microscopy (SEM and TEM respectively), XPS, and EDAX. All arsenides made by this method gave solid product except CrAs, which formed a black suspension.

CHARACTERIZATION OF BINARY ARSENIDES

The synthesized product was finely ground and used for powder X-ray diffraction (pxrd) with diffractometer scanning from 5˚ to 90˚. A Tecnai F20 microscope operating at 200 kV was used for TEM while a dual beam Helios FIB microscope was used for SEM and STEM studies. Samples for TEM and STEM were made by dispersing these

synthesized arsenide nanoparticles in ethanol by ultra-sonication for 30 mins and adding drops from this diluted dispersion on a carbon coated 200 mesh Cu TEM grid followed by drying in air.

SQUID studies were performed to measure field-dependent isothermal magnetization and temperature-dependent magnetic moment at constant field. The powdered sample of 13.1 mg of FeAs and 16.9 mg of CoAs was loaded in a gel cap and inserted into the magnetometer. Background data was collected from the diamagnetic gel cap separately and subtracted from the sample signal. The isothermal magnetization at various temperature (5K, 100K, and 300 K) was collected by varying applied magnetic field from -20,000 Oe to 20,000 Oe and reported the change in sample magnetization.

Figure A2 (a) shows the pxrd pattern of FeAs nanoparticles, and is compared with the standard reference in JCPDS file 01-076-0458. These nanoparticles were found to be highly crystalline. A TEM image is shown in Figure A2.
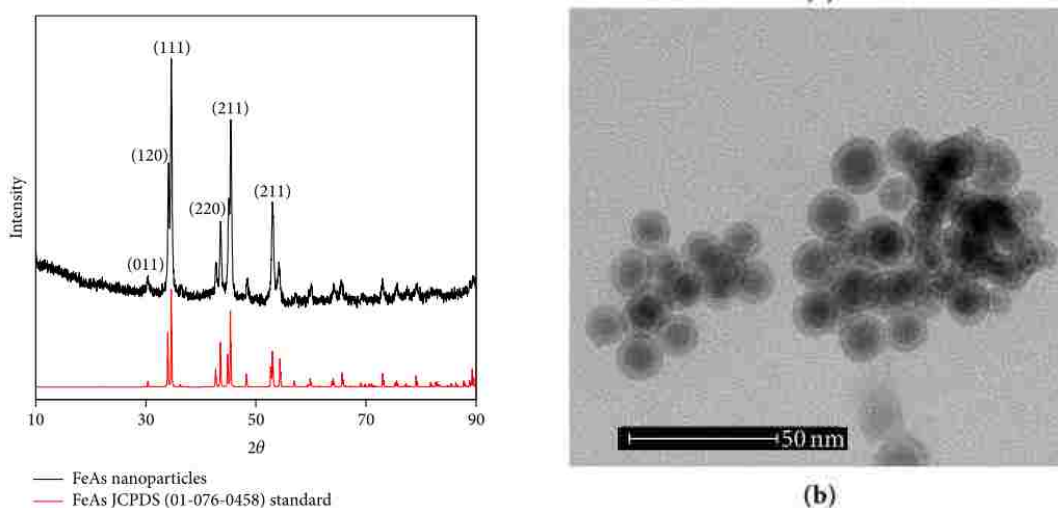

Figure A2. (a) pXRD of FeAs nanosparticles, (b) TEM of FeAs

From Figure A3, the pXrd pattern suggest that pure-phase CoAs nanostructures (JCPDS -01-077-1351) were formed and Figure A3 (b) shows the TEM image of CoAs nanorod indicating crystalline growth. The probability of nanowire formation is higher in CoAs. In the case of CoAs, hot-injection method gave rise to 1D nanostructures within first 10 mins of $Co_2(CO)_8$ introduction to the mixture. As the reaction proceeded for another 40 mins, longer CoAs nanorods with uniformity was obtained.
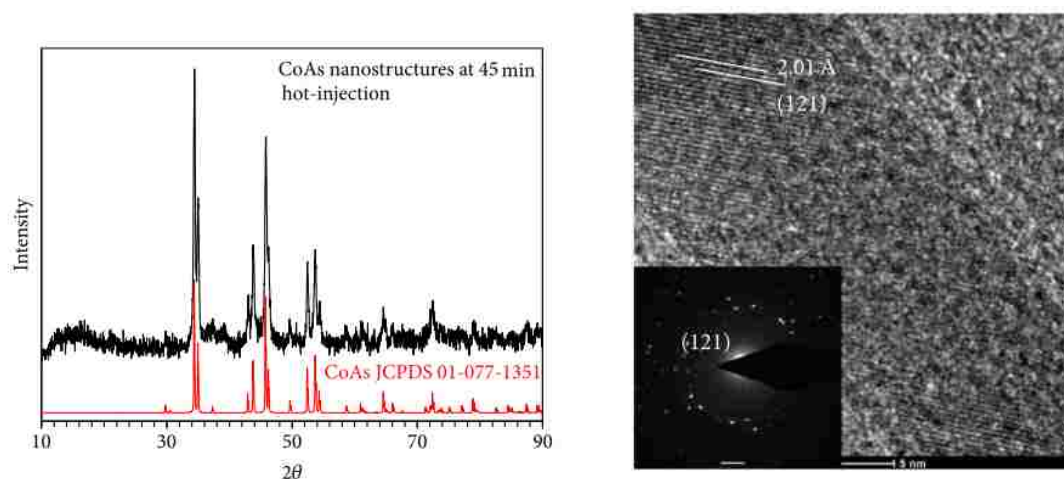

Figure A3. (a) pXRD of CoAs, (b) TEM of CoAs nanorods

MnAs nanoparticles were obtained by reacting manganese carbonyl with TPA and the pXrd pattern figure shows that JCPDS-0072-1065 was formed with Mn_3As in small trace as impurity which was picked up by pXrd. Figure A4 (b) shows STEM image of MnAs nanoparticle revealed the size range to be 5 to 10 nm. These MnAs nanoparticles

are considerably smaller compared to FeAs and CoAs. MnAs nanoparticles have magnetostructural properties and are known to have electromotive force.
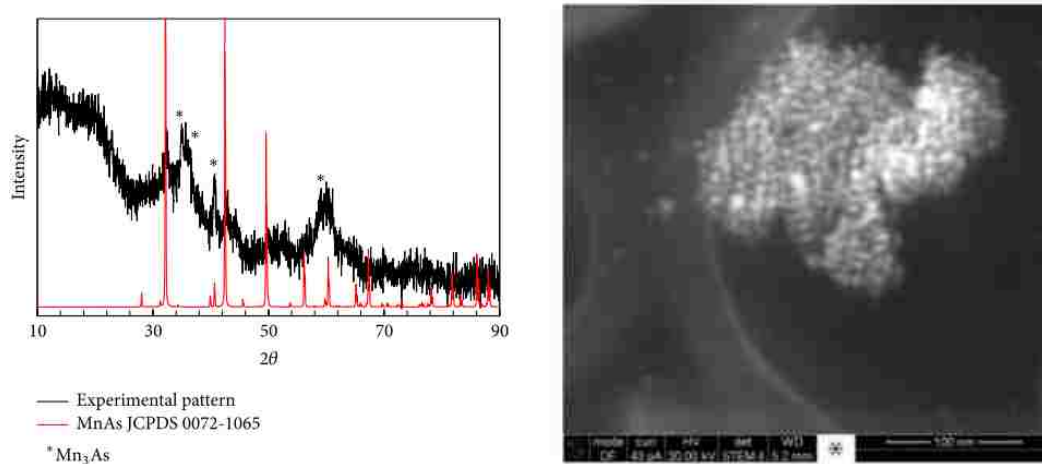

Figure A4 (a) pXRD of MnAs, (b) TEM of MnAs nanoparticles

CrAs is a ferromagnetic semiconductor and in this synthesis process it was very difficult to isolate the product in the form of a dry product because of its small size and it is well dispersed in solvents. In order to characterize, TEM, EDS and UV-Vis spectroscopy were conducted. PXRD pattern could not be conducted because of very small quantity and lack of dry powder. Figure A5 (a) shows HRTEM image of CrAs nanoparticles or quantum dots. Both TEM and EDS confirm the particle morphology and composition. Figure A5 (b) shows the absorption spectrum of CrAs nanoparticle and a strong absorption peak at 560 nm was observed and a band gap of 1.9 eV was estimated from the absorption edge. In this case, the nature and peak positions of the absorption spectra indicate to be CrAs

nanoparticle and considerable quantum confinement in the nanoparticles resulted in a blue shift of the absorbance band.
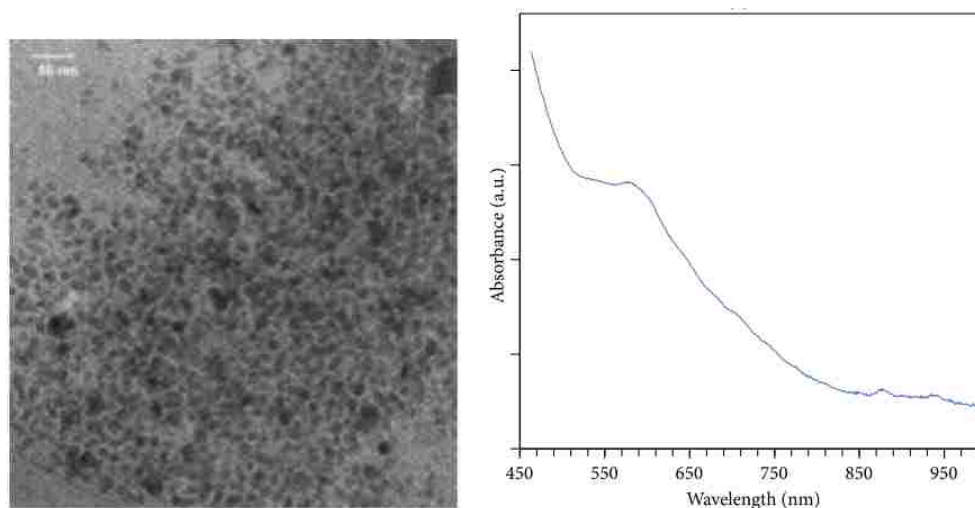

Figure A5. (a) TEM image of CrAs nanostructure, and (b) the UV-Vis spectra

Transition metal arsenides are known for their novel magnetic properties and nanostructured transition metal arsenides also exhibit interesting magnetic properties. Magnetic properties of FeAs and CoAs nanostructures were measured using temperature-dependent and field-dependent magnetization plots implying these nanoparticles to be superparamagnetic with high blocking temperature (T_B). CoAs nanostructures show ferromagnet-like ordering at low temperature attributing to their anisotropic shape as in Figure A6. Prediction has been made that when superparamagnetic T_B can be increased by increasing the shape anisotropy. Higher T_B along with larger coercivity increases the applicability of these nanostructures making them suitable for magnetic memory storage

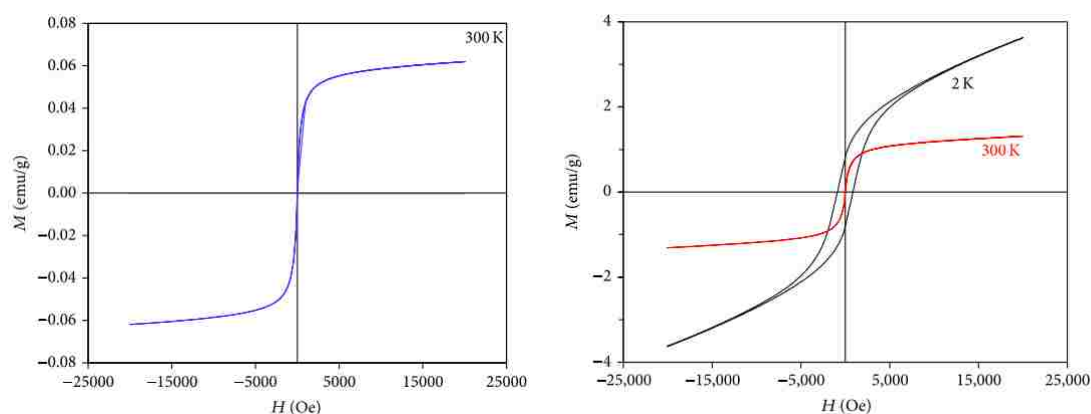and related devices, and the ability to tune T_B through subtle variation in the synthesis methodology.

Figure A6**.** Anhysteretic isothermal magnetization showing the superparamagnetic nature of the (a) FeAs and (b) CoAs.

In general, we observed that the propensity towards the formation of 1-D nanostructures increases as the d electrons availability increases (Cr to Co). CoAs forms nanorods whereas MnAs and FeAs form nanoparticles and CrAs form extremely small quantum dots. This may be due to several factors like stability/reactivity of acid-base adduct-like intermediate formed through ligand exchange, growth-rate of the nuclei, and the rate conversion. A facile one-step precipitation method to synthesize monoarsenides of 3d transition element involving very simple redox reaction between the metal carbonyl and the arsine precursors with the help of amine surfactant to provide a slightly basic medium. The morphology evolution of the product nanostructures across the transition metal series was observed and concluded that reaction kinetics plays an influential role.

BIBLIOGRAPHY

1.   Romain . S; Vigara . L; Llobet . A; Acc. Chem. Res. 2009, 42, 1944-1953.

2.   Concepcion, J.J.; Jurss, J.W.; Brennaman, M.K.; Hoertz, P.G.; Patrocinio, A.O.T.; Murakami Iha, N.Y.; Templeton, J.L.; Meyer, T.J., Acc. Chem. Res 2009,42,1954-1965.

3.   Haussener, S.; Xiang, X.; Spurgeon, J.M.; Ardo, S.; Lewis, N.S.; Weber, A.Z., Modeling, simulation, and design criteria for photochemical water-splitting. Energy. Environ.Sci., 2012, 5, 9922-9935.

4.   Modestino, M.A.; Walczak, K.A.; Berger, A.; Evans, C.M.; Newman, J.A.; Ager, J.W.; Segalman, R.A., Robust production of purified H_2 in a stable, self-regulating and continuously operating solar fuel generator. Energy.Environ.Sci, 2013, 7, 297-301.

5.   Newman, J., Scaling with ohm's law; wired vs. wireless photochemical cells. J.Electrochem. Soc.,2013, 160, F309-F311.

6.   Brimblecombe,R.; Dismukes,G.C; Swiegers,G.F.;Spiccia,L.; Molecular water-oxidation catalysts for photochemical cells. Dalton Transactions, 2009, 43, 9374-9384.

7.   Yan, Y., Xia, B.Y., Ge X., Liu Z., Fisher A., Wang X.; A Flexible Electrode Based on Iron Phosphide Nanotubes for Overall Water splitting. Chem. Eur. J, 2015, 21, 1-7.

8.   Li,S.; Van Zee, R.J.; Weltner,W., Far-infrared spectra of small gallium phosphide, arsenide, and antimonide molecules in rare-gas matrixes at 4K. J.Phys.Chem. 1993, 97, 11393-11396.

9.   Assali,S.; Zardo,I.; Plissard,S.; Meijerink,A.; Belabbes,A.; Bechstedt,F.; Haverkort,J.E.M.; bakkers,E.P.A.M., Direct band gap Wurtzite Gallium phosphide nanowires. Nano Lett. 2013, 13, 1559-1563.

10. Henkes,A.E.; Schaal,R.E., Trioctylphosphine: A general phosphorous source for the low-temperature conversion of metals into metal phosphide. Chem.Mater. 2007, 9, 4234-4242.

11. Nozik,A.J.; Beard,M.C.; Luther, J.M.; Ellingson,R.J.; Johnson ,J.C., Semiconductor Quantum Dots and Quantum Dot arrays and applications of multiple Exciton Generation to third-generation photovoltaic solar cells. Chem.Rev. 2010, 110, 6873-6890.

12. Muthuswamy,E.; Kharel,P.R.; Lawes,G.; Brock,S.L., Control of phase in phosphide nanoparticles produced by metal nanoparticle transformation: Fe_2P and FeP. ACS Nano 2009, 3, 2383-2393.

13. Perera,S.C.; Tsoi,G.; Wenger,L.E.; Brock,S.L., Synthesis of MnP nanocrystals by treatment of metal carbonyl complexes with phosphines: A new versatile route to nanoscale transition metal phosphides. J.Am.Chem.Soc., 2003, 125, 13960-13961.

14. Perera,S.C.; Tsoi,G.; Wenger,L.E.; Brock,S.L., Synthesis of MnP nanocrystals by treatment of metal carbonyl complexes with phosphines: A new versatile route to nanoscale transition metal phosphides. J.Am.Chem.Soc., 2003, 125, 13960-13961.

15. Senevirathne,K.; Burns,A.W.; Bussell,M.E.; Brock,S.L., Synthesis and characterization of discrete nickel phosphide nanoparticles: effect of surface ligation chemistry on catalytic hydrodesulfurization of the thiophene. Adv.Funct.Mater., 2007, 17, 3933-3939.

16. Perera,S.C.; Tsoi,G.; Wenger,L.E.; Brock,S.L., Synthesis of MnP nanocrystals by treatment of metal carbonyl complexes with phosphines: A new versatile route to nanoscale transition metal phosphides. J.Am.Chem.Soc., 2003, 125, 13960-13961.

17. Nozik,A.J.; Beard,M.C.; Luther, J.M.; Ellingson,R.J.; Johnson ,J.C., Semiconductor Quantum Dots and Quantum Dot arrays and applications of multiple Exciton Generation to third-generation photovoltaic solar cells. Chem.Rev. 2010, 110, 6873-6890.

18. Kamaihara,Y.; Hiramatsu,H.; Hirano,M.; Kawamura,R.; Yanagi,H.; Kamiya,T.; Hosono,H., Iron-based layered superconductor: LaOFeP. J.Am.Chem.Soc, 2006, 128, 10012-10013.

19. Balli,M.; Fruchart,D.; Gignoux,D.; Zach,R., The "colossal" magnetocaloric effect in $M_{1-x}Fe_xAs$: what are we really measuring?, Appl.Phys.Lett., 2009, 95, 072509-072509-3.

20. Shem,B.; Sun,J.; Hu,F.; Zhang,H.; Cheng,Z., Recent progress in exploring magnetocaloric materials. Adv.Mater. 2009, 21, 4545-4564.

21. Imai,M.; Akaishi,M.; Sadki,E.; Aoyagi,T.; Kimura,T.; Shirotani,I., Superconducting properties of filled skutterudite $La_{0.8}Rh_4P_{12}$. Phys.Rev.B, 2007, 75, 184535.

22. Ivanovskii,A.L., New high-temperature superconductor based on rare-earth and transition metal oxyarsenides and related phases/; Synthesis, properties and simulations. Phy Usp. 2008, 51, 1229.

23. Goodenough, J., Interpretation of structure and magnetism in transition-metal pnictides M_2X and $(M_{1-x} M^{'}_x)_2$ X. J.Solid State Chem. 1973, 7, 428-447.

24. Li,Y.; Malik,M.A.; O'Brien,P., Synthesis of single-crystalline CoP nanowires by a one-pot metal organic route. J.Am.Chem.Soc. 2005,127, 16020-16021.

25. Zhang,H.; Ha,D.-H.; Hovden,R.; Kourkoutis,L.F.; Robinson,R.D., Controlled synthesis of uniform cobalt phosphide hyperbranched nanocrystals using Tri-n-octylphosphine oxide as a phosphorous source. Nano Lett. 2010, 11, 188-197.

26. Chiang,R.-K.; Chiang,R.-T., Formation of Hollow Ni_2P nanoparticles based on the nanoscale kirkendall effect. Inorg.Chem. 2006, 46, 369-371.

27. Barry,B.M.; Gillan,E.G., Low-temperature solvothermal synthesis of phosphorius-rich transition-metal phosphides. Chem.Mater., 2008, 20, 2618-2620.

28. Stamm,K.L.; Garno,J.C.; Liu.G.-y.; Brock,S.L., A general methodology for the synthesis of transition metal pnictide nanoparticles from pnictate precursors and its application to iron phosphorus phases. J.Am.Chem.Soc. 2003, 125, 4038-4039.

29. Zhang,X.M.; Wang,C.; Qian,X.F.; Xie,Y.; Qian,Y.T., Synthesis of nanocrystaliine iron monoarsenide via a reductive recombination pathway. J.Solid state Chem, 1999, 144, 237-239.

30. Wang,J.; Yang,Q., A developed Ullmann reaction to III-V Semiconductor nanocrystals in sealed vacuum tubes. Dalton Transactions 2008, 43, 6060-6066.

31. Xie,Y.; Lu,J.; Yan,P.; Jiang,X.; Qian,Y., A safe low temperature route to nanocrystaliine transaction metal arsenides. Chem.Lett. 2000, 114-115.

32. Klingan,F.; Robert,X.; Miehr,A.; Fischer,R.A.; Herrmann,W.A., Thin films of CoAs from low temperature metalorganic chemical vapor deposition of a novel single; source precursor compound. Appl.Phys.Lett.1995, 67, 822-824.

VITA

Nikitaa Ashokan was born on September 14, 1990 in Chennai, India. She obtained her undergraduate degree in Chemical Engineering from Amrita University, Coimbatore, India in 2012. In her senior year, she worked on her thesis project on "Performance enhancement of Cogeneration cycles using Microchannel Heat Exchanger", under the supervision of Dr. Uday Baskar Reddy. Her work was to fabricate microchannel heat exchanger and compare the CHP cycles performance by replacing the conventional heat exchanger with microchannel heat exchanger using ASPEN HYSYS. After her under-graduation, in Spring 2013 she started her masters in Chemical Engineering at Missouri University of Science and Technology (Missouri S&T), Rolla, Missouri.

At Missouri S&T, she did her research work on synthesizing a suitable electrochemical water splitting catalyst and did electrochemical studies. She received her Masters in Chemical Engineering from Missouri S&T in May, 2016.